

High-coherence mid-infrared dual-comb spectroscopy spanning 2.6 to 5.2 μm

Gabriel Ycas ^{*}, Fabrizio R. Giorgetta, Esther Baumann, Ian Coddington, Daniel Herman, Scott A. Diddams and Nathan R. Newbury

Mid-infrared dual-comb spectroscopy has the potential to supplant conventional Fourier-transform spectroscopy in applications requiring high resolution, accuracy, signal-to-noise ratio and speed. Until now, mid-infrared dual-comb spectroscopy has been limited to narrow optical bandwidths or low signal-to-noise ratios. Using digital signal processing and broadband frequency conversion in waveguides, we demonstrate a mid-infrared dual-comb spectrometer covering 2.6 to 5.2 μm with comb-tooth resolution, sub-MHz frequency precision and accuracy, and a spectral signal-to-noise ratio as high as 6,500. As a demonstration, we measure the highly structured, broadband cross-section of propane from 2,840 to 3,040 cm^{-1} , the complex phase/amplitude spectra of carbonyl sulfide from 2,000 to 2,100 cm^{-1} , and of a methane, acetylene and ethane mixture from 2,860 to 3,400 cm^{-1} . The combination of broad bandwidth, comb-mode resolution and high brightness will enable accurate mid-infrared spectroscopy in precision laboratory experiments and non-laboratory applications including open-path atmospheric gas sensing, process monitoring and combustion.

Mid-infrared spectroscopy is a powerful technique for the multispecies detection of trace gases, with applications ranging from the detection of hazardous materials to environmental monitoring and industrial monitoring. Compared to the near-infrared, where laser sources are more plentiful, the techniques for measuring mid-infrared spectra are more limited. Mid-infrared spectra are most commonly acquired by Fourier-transform spectroscopy (FTS), which provides accurate and high-resolution spectra, but requires a scanning delay arm and blackbody source. This leads to large instruments and long acquisition times. Dual-comb spectroscopy (DCS) is a high-performance alternative to conventional FTS, providing high resolution, absolute frequency accuracy, fast acquisition times, long interaction lengths, broad bandwidth coverage and high signal-to-noise ratio (SNR)^{1,2}. The advantages of speed and long path length are of particular relevance to non-laboratory applications, for example in open-path atmospheric monitoring or industrial process monitoring^{3–6}. However, until now, DCS has only been demonstrated with its full panoply of advantages in the near-infrared, from ~ 1 to 2 μm (refs 7–10). The near-infrared has much more limited applications compared to the mid-infrared, because molecular cross-sections are typically 1,000 times weaker, if they exist at all. DCS in the mid-infrared has indeed been actively pursued^{11–24}, yet it is not competitive with high-resolution conventional FTS, being limited by the coherence and/or bandwidth of mid-infrared comb sources.

For quantitative broadband mid-infrared DCS, the strong overlapping requirements for the underlying mid-infrared frequency combs must be addressed: they must produce broad and relatively flat optical spectra while maintaining mutual coherence over the measurement time. Without coherence, adjacent comb teeth blend together, sacrificing orders of magnitude in spectral resolution and obscuring both the frequency and amplitude accuracy possible with this technique. The requirements for bandwidth and coherence are strongly coupled—as the optical bandwidth increases (or required SNR increases), the measurement time must correspondingly increase, putting ever more stringent requirements on the mutual

coherence between the combs. Driven by the challenges involved in generating highly coherent mid-infrared light, high-SNR, accurate and quantitative mid-infrared DCS has so far been limited to narrow instantaneous bandwidths^{13,17,20}.

In this Article, we demonstrate mid-infrared dual-comb spectroscopy with high coherence, recording a high-fidelity spectrum of the complex molecule propane. We capture both the broad 200 cm^{-1} pedestal and complicated fine structure of this gas, which has features as narrow as 0.01 cm^{-1} (300 MHz). We demonstrate that high-coherence DCS spectra of large molecules can have fidelity equivalent to high-resolution FTS spectra, without requiring correction for instrument lineshape or frequency calibration, with a faster acquisition time and in a more compact footprint compatible with future non-laboratory use. We also measure the spectrum of a gas mixture of methane, acetylene, carbonyl sulfide (COS), ethane and water, measuring the complex (phase and amplitude) spectra in both the 3 μm region and 5 μm region, spanning the entire L and M atmospheric transmission windows.

Data processing for comb-tooth-resolved spectra

Multiple approaches have been taken to achieve the mutual comb coherence needed for dual-comb spectroscopy, but often at the cost of bandwidth or experimental complexity¹. Of these approaches, digital signal processing alone can avoid these trade-offs while enforcing not only mutual coherence but also enabling the coherent averaging needed to acquire high-SNR spectra. Real-time phase correction through digital signal processing has only been demonstrated so far in a relatively narrow optical region around a pair of c.w. lasers acting as transfer oscillators^{7,30}. We generalize the digital signal-processing approach to support broadband DCS by allowing for the correction of a DCS signal at any colour using an arbitrary pair of optical references, demonstrated by our use of two near-infrared signals to correct a mid-infrared DCS signal.

We implement real-time phase correction on a field-programmable gate array (FPGA). The FPGA signal processor also implements coherent averaging, critical to reducing the data size for any

reasonable averaging time³¹. As described in the Methods, each interferogram first undergoes real-time phase/timing corrections and is then added point by point to a running summed interferogram. This process is repeated to average up to 65,000 interferograms on the FPGA, at which point they are transmitted to a PC over a RIFFA interface³².

Figure 2 shows a series of coherent, comb-tooth-resolved spectra for tuning of the PPLN from 2.6 to 5.2 μm . For each spectrum, 69 interferograms with 1,922,334 samples each were recorded in 0.66 s and then Fourier-transformed to produce optical spectra. We observe resolved DCS comb modes with no signs of line broadening at all spectral bands, demonstrating that for all mid-infrared spectra the relative comb linewidth is less than 2 Hz. For longer acquisitions we implement coherent averaging as described in the Methods, which effectively retains only the (complex) values at the DCS radiofrequency comb teeth, to generate high-SNR spectra as shown in Fig. 1b and in the remainder of this Article. With coherent averaging, the SNR improves as the square root of time, essentially indefinitely (Fig. 1b and Supplementary Fig. 1). The coherently averaged spectra are sampled at an optical 200 MHz point-spacing (the comb repetition rate) where each sample has a frequency accuracy of 100 kHz, set by the fractional uncertainty of the counted repetition rates, and a linewidth less than 1 MHz, determined by the absolute linewidth of the frequency combs. Figure 2c shows a high-resolution spectrum of several well-characterized ~ 300 MHz-wide, hydrogen cyanide (HCN) absorption lines^{33,34}.

The digital signal-processing system presented here can be applied to almost any dual-comb spectroscopy system, and provides a technically simple means of achieving mutual optical coherence between a pair of combs. Significantly, the signal-processing system does not rely on any relationship between the two optical locking frequencies and the frequency of the dual-comb signal; for example, the same signal processor should function equally well with two telecom-band c.w. lasers and a visible-light interferogram.

Mid-infrared frequency combs

Our mid-infrared laser frequency combs use difference frequency generation (DFG) to convert near-infrared light into 2,600–5,200 nm mid-infrared light, as shown in Fig. 1. Each system is based on a self-referenced polarization-maintaining fibre frequency comb with a repetition rate of 200 MHz (ref. 25). The lasers are stabilized by phase-locking a comb tooth to a common cavity-stabilized 1,560 nm continuous-wave (c.w.) laser and the carrier-envelope offset frequency to a fraction of the repetition frequency. The resulting stabilized repetition rate is then counted against a radiofrequency reference, here a hydrogen maser, to provide absolute frequency calibration. The near-infrared comb output is preamplified to about 30 mW and then split equally into three branches. The first branch generates the $f-2f$ signal used to lock the comb's offset frequency. The second branch generates pump light for the DFG process at 1,070 nm. The preamplifier output is amplified in a core-pumped erbium-doped fibre amplifier (EDFA) and launched into a highly nonlinear optical fibre (HNLF) with anomalous dispersion. This provides about 1 mW of power between 1,040 and 1,090 nm, which is filtered, stretched with a chirped fibre Bragg grating, amplified to 1.6 W in an ytterbium-doped fibre amplifier, and compressed with a Treacy compressor to ~ 200 fs and 900 mW of average power. The third branch generates signal light spanning 1,350 to 1,750 nm by amplification in a core-pumped EDFA to 430 mW and subsequent broadening in normal-dispersion HNLF.

Light from the pump and signal branches is combined on a dichroic mirror and focused into a periodically poled lithium niobate (PPLN) crystal using an off-axis paraboloid mirror. We have used both a bulk PPLN crystal 1 mm in length^{14,17,19,26,27} and a chirped PPLN waveguide. The chirped waveguide PPLN generates a structured but broad spectrum with an instantaneous bandwidth

exceeding 1,600 cm^{-1} . The bulk crystal provides smoother spectra with optical bandwidths from 760 to 120 cm^{-1} (-10 dB) as the centre wavelength is tuned from 3 to 5 μm by selecting different poling periods, as shown in Fig. 2. The output powers range from 40 to 100 mW for wavelengths from 2.5 to 3.8 μm and from 1 to 10 mW for wavelengths from 4 to 5 μm , sufficient to support future open-path measurements. For the laboratory data here, the mid-infrared light is attenuated to a few hundred microwatts to avoid saturation of the HgCdTe detector.

The choice of DFG for the mid-infrared combs is not the only option. In addition to DFG, other mid-infrared DCS demonstrations have emphasized novel sources such as quantum cascade lasers^{23,28}, femtosecond lasers¹², microresonators²¹ and optical parametric oscillators^{15,18,22,24}. The DFG combs have a combination of attributes that are attractive. First, the combs' phase noise can be measured easily in the near-infrared and then extrapolated to the mid-infrared region. Second, the DFG combs can provide powers up to 100 mW, more than sufficient for operation in stressing, long-path configurations. Third, the DFG process is relatively simple, so the combs operate continuously for many days. Finally, the entire system can easily fit on a 3' \times 5' table. Therefore, by slightly modifying the locking scheme to follow ref. 29, the entire mid-infrared DCS optical system can be made portable for non-laboratory use where the improvements of mid-infrared DCS over conventional high-resolution FTS would have the most impact.

Results

Propane absorption cross-section. In contrast to previous DCS demonstrations, which have focused on narrow absorption features, we measure the 200 cm^{-1} wide absorption cross-section of low-pressure propane gas. Propane was chosen due to its broad absorption feature at 3.4 μm , which is qualitatively similar to the spectra of other large organic molecules, and also for its relevance to air quality and oil- and gas-monitoring efforts³⁵. Accurately measuring the absorption cross-section requires high resolution to capture the fine structure, as well as a flat spectral response over a wide bandwidth to capture the broader absorption pedestal.

A gas cell was constructed with wedged CaF_2 windows to avoid etalon effects, and filled with propane gas at low pressure. The mid-infrared comb spectra, generated here in a bulk PPLN crystal, change slowly with time, so a signal spectrum I_{sig} and reference spectrum I_{ref} were measured simultaneously, as shown in Fig. 3a,b. A static discrepancy between them was calibrated out by recording the pair $I_{\text{sig}}^{\text{cal}}$ and $I_{\text{ref}}^{\text{cal}}$ after purging the gas cell with ambient air. We calculated the normalized transmission as $T_{\text{propane}} = (I_{\text{sig}}^{\text{cal}} / I_{\text{ref}}^{\text{cal}}) / (I_{\text{sig}} / I_{\text{ref}})$ and then the molecular absorption cross-section as

$$\sigma = -\ln(T_{\text{propane}}) \times \frac{k_{\text{B}}T}{pL} \quad (1)$$

where the cell length is $L = 36$ cm, the propane pressure is $p = 1$ torr, and the room temperature is $T = 293$ K. As shown in Fig. 3c,d, the measured cross-section agrees well with a recent high-resolution FTS measurement³⁶, capturing both a broad absorption envelope and many narrow features. The statistical uncertainty of the cross-section scales inversely with the signal strength of the raw spectra, being $\sim 1 \times 10^{-21} \text{ cm}^2 \text{ molecule}^{-1}$ at 2,967.6 cm^{-1} and $\sim 0.25 \times 10^{-21} \text{ cm}^2 \text{ molecule}^{-1}$ at 2,900 cm^{-1} . The FTS and DCS spectra agree well, as shown, and have a similar SNR of 2,000:1 based on the point-to-point fluctuations in the wings of the cross-section (where variations in the actual cross-section do not dominate the point-to-point scatter). However, the FTS measurement time is 12 h, while the DCS spectra were acquired in 182 min, or about four times faster. Of course, any generalized comparison of acquisition speed between the DCS and high-resolution FTS has many qualifiers.

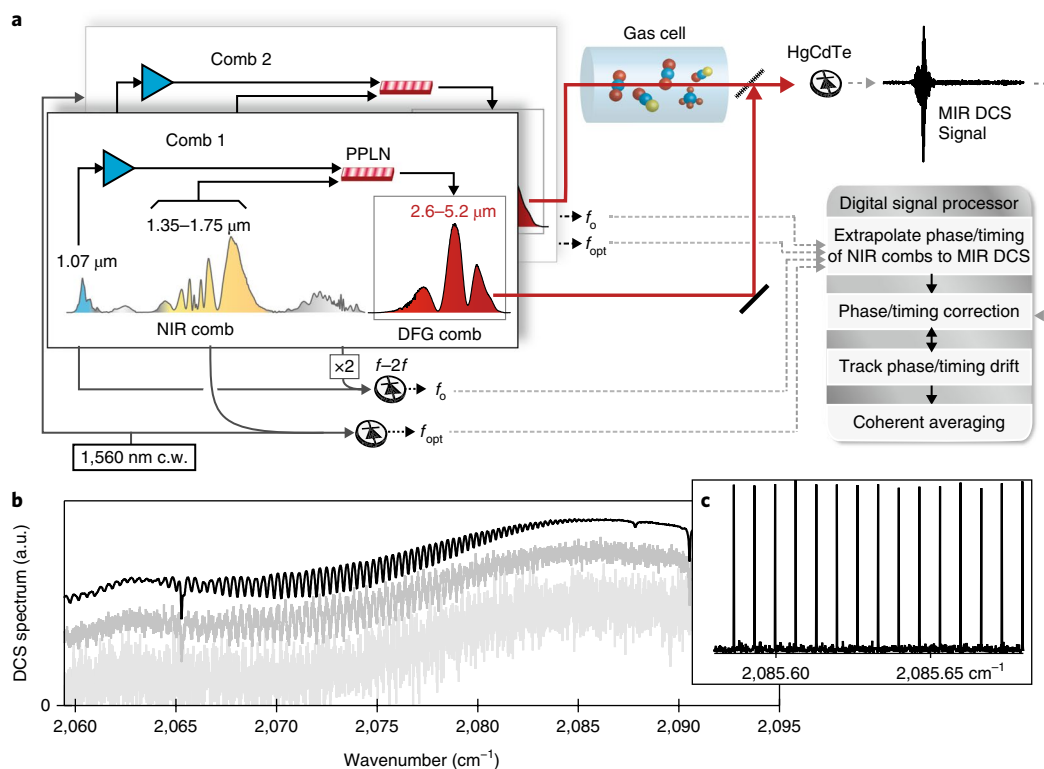


Fig. 1 | Octave-spanning mid-infrared dual comb spectrometer. **a**, Near-infrared laser frequency combs generate mid-infrared light by DFG in bulk or chirped waveguide PPLN. Light from one comb is passed through a gas cell and combined with the second comb to generate a series of interferograms that are detected on a mercury-cadmium-telluride (HgCdTe) photodetector. A digital signal processor corrects the phase and timing of the detected interferograms based on the instantaneous near-infrared combs' offset frequencies, f_o , and optical comb tooth frequencies near 1,560 nm, f_{opt} , as well as slower environmentally driven phase/timing drifts from the other optical subsystems. The Fourier transform of these corrected interferograms yields the mid-infrared spectrum. **b**, Example mid-infrared spectrum of COS near 5 μm ($2,000\text{ cm}^{-1}$) at coherent averaging times of 10 ms (light grey), 100 ms (dark grey) and 100 s (black), illustrating the expected improvement in SNR with coherent averaging time. **c**, Example comb-tooth resolved spectrum in the same spectral region for 600 ms of streamed phase/timing-corrected DCS data. NIR, near-infrared; MIR, mid-infrared.

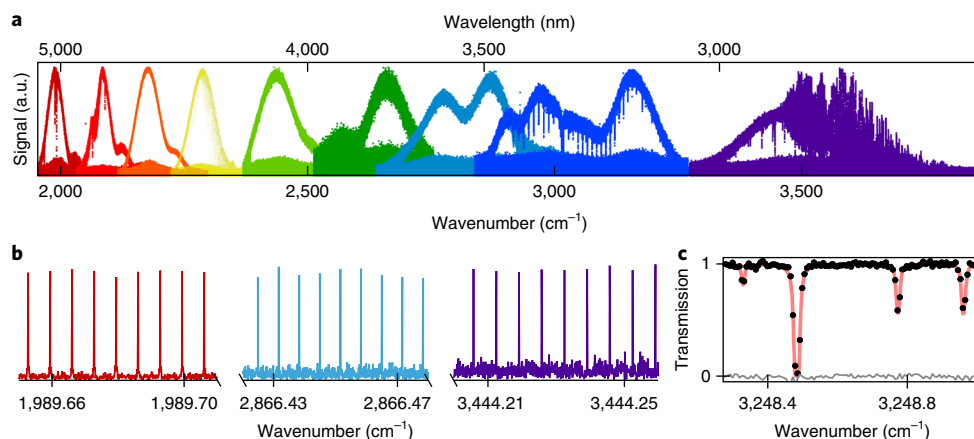


Fig. 2 | Dual-comb spectra. **a**, Dual-comb spectra at different PPLN poling periods, for ~ 0.6 s of streamed, phase- and timing-corrected DCS data. The spectra span $\sim 1,800\text{ cm}^{-1}$ bandwidth or 270,000 resolved comb modes. They have been normalized to equal peak height. The structure above $3,500\text{ cm}^{-1}$ (ref. 11) is due to water absorption in ambient air. **b**, Expanded view showing resolved comb modes spaced by 0.0067 cm^{-1} (200 MHz) across the covered spectral range. These spectra are shown before coherent averaging, which only retains the values at the DCS comb teeth. **c**, Expanded view of a coherently averaged DCS spectrum for a 2.6 torr cell of hydrogen cyanide (HCN). The DCS is sampled at 200 MHz comb tooth spacing, as indicated by the black dots, and falls directly on the HCN spectra from refs 33,34 (red line).

On the one hand, the DCS acquisition speed, for a given SNR, could be increased 200 times if one eliminated the noise floor due to the relative intensity noise of the combs, through either comb

design or balanced detection. On the other hand, the required DCS acquisition time increases with optical bandwidth³⁷, and in this comparison, the bandwidth of the DCS was less than the

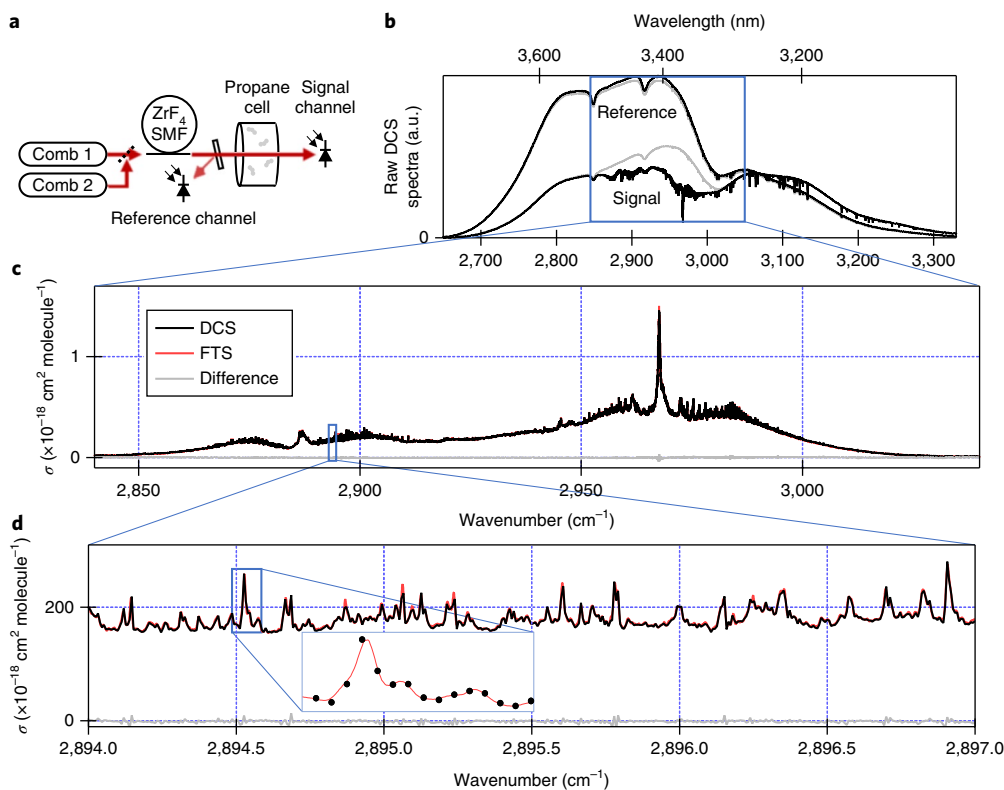


Fig. 3 | Propane spectrum and cross-section. **a**, For the propane measurement, the light of both combs is combined on a 50:50 splitter and sent through a single-mode ZrF_4 fibre. A wedged window samples the beam to provide a reference, and the remainder of the light probes the propane cell. A second window (not shown) is used to sample the light transmitted through the propane cell, to avoid saturation of the photodetector. **b**, Raw DCS spectra with the signal channel probing the cell filled with propane (black) and the empty cell (grey), spanning 700 cm^{-1} and $100,000$ teeth. **c**, Propane cross-section σ , extracted from the normalized DCS spectra. The DCS measured cross-section, spanning 200 cm^{-1} and $30,000$ comb modes, compares well to a high-resolution FTS measurement by Beale et al.³⁶ (red line), with their difference (grey line) flat to within $3 \times 10^{-21}\text{ cm}^2\text{ molecule}^{-1}$ (standard deviation). **d**, Detail of the propane cross-section, showing its highly structured nature and excellent agreement between the DCS and high-resolution FTS. As further magnification shows, the width of some of the narrower spikes are around 0.01 cm^{-1} , compared to the comb tooth spacing of 0.0067 cm^{-1} .

FTS. Indeed, in the laboratory setting, high-resolution FTS is well known to provide high-SNR spectra in sufficient acquisition times. However, and most importantly, the DCS uses high-brightness comb light, which was attenuated here 20-fold to avoid detector saturation. Therefore, the same acquisition speed and SNR should be achievable with this DCS even if the sample region has a much higher effective insertion loss (for example, as with a kilometre-long atmospheric path or lossy combustion chamber), whereas the SNR for a high-resolution FTS would suffer from low signal in such cases (with the notable exception of solar-looking FTS). Finally, no instrument lineshape correction, baseline correction or separate frequency axis calibration was needed for the DCS data. These data represent the first quantitative comparison between a broad, structured spectrum measured via conventional high-resolution FTS and via DCS.

Complex (phase and absorption) spectra of gas mixtures. In a second measurement, the set-up was configured as shown in Fig. 1a and the gas cell was filled with a mixture of 5,000 ppm methane (CH_4), 1,000 ppm COS, 5,000 ppm acetylene (C_2H_2) and 500 ppm ethane (C_2H_6) buffered with nitrogen at atmospheric pressure. Spectra were acquired at two different spectral bands by selecting the poling period of the bulk PPLN crystal.

Figure 4 shows the measured spectrum over $2.9\text{--}3.6\text{ }\mu\text{m}$, corresponding to a bandwidth of 650 cm^{-1} (20 THz) and $100,000$ resolved comb modes. Spectra were coherently averaged for 32 min, achieving a peak spectral SNR—defined as the ratio of the signal to the

random variations of the baseline—of 660 or $15/\sqrt{5}$. The overall comb intensity structure was removed using standard baseline fitting techniques to find the transmission and phase spectra shown, which agree well with a model based on HITRAN 2008 line parameters and Voigt lineshapes³⁸, as is also seen even more strongly in the comparison with the narrow, well-calibrated HCN lines in Fig. 2c. Indeed, we attribute any slight differences in Fig. 4 to the HITRAN 2008 database, illustrating the potential of mid-infrared DCS to contribute to improved spectral databases.

Figure 5 shows the measured spectrum at longer wavelengths from 5.08 to $4.75\text{ }\mu\text{m}$, corresponding to a bandwidth of 136 cm^{-1} (4.1 THz) and $20,000$ resolved comb modes. Spectra were coherently averaged for 80 min, achieving a peak spectral SNR of $6,500$, or $94/\sqrt{5}$. As before, the phase and transmission spectra were extracted after standard baseline correction for the comb structure and agree very well with the HITRAN 2008 based model.

We can compare different spectra and dual-comb systems through a DCS figure of merit³⁷, defined as the average SNR (not peak) times the number of comb modes, which is then identical to simply summing the SNR across the comb modes (see Methods). The SNR refers to the uncorrelated point-to-point spectral fluctuations and ignores slower variations from, for example, any changing etalons in the beam paths. We find a figure of merit of $1.5 \times 10^6/\sqrt{5}$ for the propane spectrum of Fig. 3 and $6 \times 10^5/\sqrt{5}$ for both the $3\text{ }\mu\text{m}$ (Fig. 4b) and $5\text{ }\mu\text{m}$ spectrum (Fig. 5a). The figures of merit are limited by the relative intensity noise (RIN) on the mid-infrared combs of approximately -127 dBc Hz^{-1} . In the future, the use of a

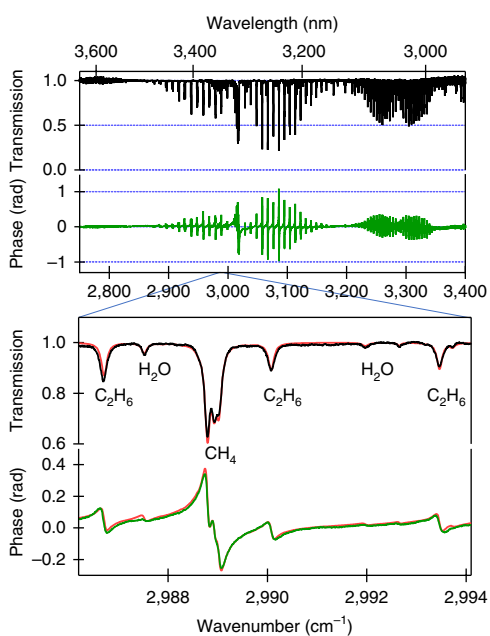


Fig. 4 | Dispersive dual-comb spectrum of gas mixture. Measured spectrum of CH₄ (methane, 2,900–3,200 cm⁻¹), C₂H₆ (ethane, ~3,000 cm⁻¹) and C₂H₂ (acetylene, ~3,300 cm⁻¹) in 1 atm of nitrogen (N₂) with a bandwidth of 650 cm⁻¹ and 110,000 comb modes. Both transmittance and phase response are shown along with the HITRAN 2008 model³⁸ (red line). Over the expanded view, the transmission noise is 0.002 and the phase noise is 2 mrad.

balanced HgCdTe detector could suppress this noise substantially, as in the near-infrared²⁹. Although these figures of merit do not reach the shot-noise limit, they are comparable to reported results for narrowband DFG DCS, which range from 1.0 to $2.3 \times 10^6 / \sqrt{s}$ (refs 13,20).

Broad instantaneous bandwidth through waveguide PPLN. Even broader instantaneous bandwidths are interesting for many applications, for example for covering the full 3–4 μm and 4.5–5 μm atmospheric windows, but are challenging to achieve in bulk PPLN crystals. To extend our interaction length while maintaining high intensities, we designed an aperiodically poled lithium niobate ridge waveguide. As shown in Fig. 6a, the waveguide has a cross-section of 15 μm × 15 μm and length of 25 mm, on a lithium tantalate (LT) substrate. Poling along the 25-mm-long waveguide is varied from periods of 22 to 30 μm to achieve phase matching for DFG from 2.6 to 5.2 μm. To mitigate the tendency of optical parametric amplification to effectively reduce the difference-frequency bandwidth, the poling period was chirped at a rate proportional to the phase-matching bandwidth, as shown in Fig. 6a. Qualitatively, less waveguide length is devoted to poling periods with broad phase-matching bandwidth, and vice versa. To generate a broad-bandwidth mid-infrared spectrum, we stretched our pump pulse to ~1 ps before coupling into the waveguide, with the final mid-infrared spectrum dependent on the relative delay between the input pump and signal light. Supplementary Fig. 2 shows one example of a smooth spectrum covering 3.2–3.7 μm at 90 mW average power, which is coupled to single-mode ZrF₄ fibre with 30% efficiency, indicating good spatial beam quality.

Figure 6b shows a DCS spectrum acquired using mid-infrared combs, each generated from chirped waveguide PPLN, with the same gas mixture of methane, ethane, COS and acetylene. While the spectra produced by the waveguide PPLN are more structured than those produced by the bulk PPLN, they are broader. The DCS

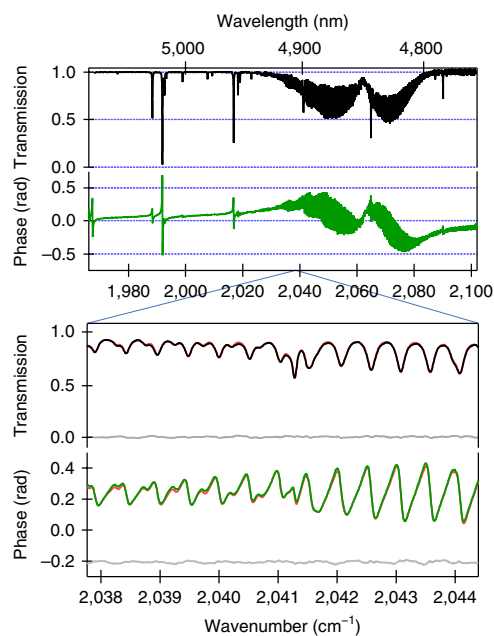


Fig. 5 | Measured spectrum of COS. Spectrum of COS in 1 atm N₂ acquired over 80 min. Both transmittance and phase response are shown along with the HITRAN 2008 model³⁸ (red line) and residuals (grey line, phase residuals offset by -0.2 rad). The spikes are H₂O lines. At 2,000 cm⁻¹, the phase noise is 200 μrad. Over the shown spectral range it averages to 4.5 mrad.

spectrum covers 2,250–3,890 cm⁻¹, corresponding to a bandwidth of 1,640 cm⁻¹ (1,874 nm and 49 THz) and 245,000 comb modes. Equally important, there is no evidence of higher intensity noise; averaging for 83 min, the spectrum achieves a peak spectral SNR of 2,000 (28/√s) and a figure of merit equal to $9 \times 10^5 / \sqrt{s}$. The retrieved gas transmission spectra agree with the HITRAN model, as shown in Fig. 6b. With further design, we anticipate that chirped-waveguide PPLNs will be able to provide high-power, single-spatial-mode, mid-infrared light with spectral coverage tailored to different broadband applications.

Discussion

Mid-infrared DCS has the potential for a much broader set of non-laboratory applications than conventional high-resolution FTS. Combining the spectral coverage of FTS and the precision of frequency combs, mid-infrared DCS has potential for high-precision lineshape studies of large molecules³⁹, high-spatial-resolution spectral microscopy⁴⁰, time-resolved spectroscopy⁴¹, combustion diagnostics⁴² and sensitive, rapid detection of large molecules even in the presence of strongly absorbing background clutter.

The system shown here is capable of comb-tooth-resolved, broadband spectroscopy in the functional group index region from 3 to 5 μm with high SNR and with frequency resolution and accuracy equal to or exceeding high-performance mid-infrared FTS. In contrast to FTS, this performance is reached with a high-power, high-brightness laser source, which is attenuated here to avoid detector saturation. Whereas traditional FTS has difficulty in lossy conditions—open-path spectrometers are typically operated at resolutions of ~1 cm⁻¹—the dual-comb spectrometer maintains its performance, thereby enabling detection over lossy open-air paths and in industrial process monitoring.

Future improvements to the dual-comb spectrometer will increase robustness, optical bandwidth and portability. With improved PPLN waveguide designs, it will be possible to generate spectra that are both broad and flat. Waveguides will also increase the DFG efficiency, lowering the required infrared optical power

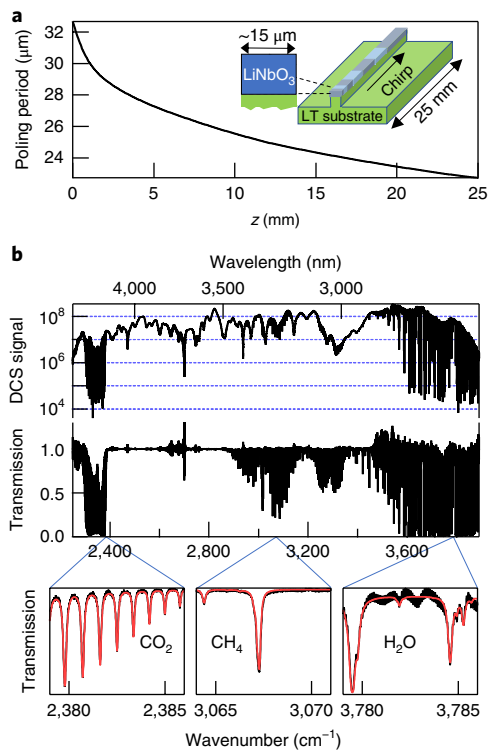


Fig. 6 | Broadband dual-comb spectroscopy with light generated in PPLN waveguides. **a**, Aperiodic poling design of the lithium niobate waveguides used, showing variation of poling periods from the waveguide entrance ($z=0$) to the exit ($z=25$ mm). Inset: waveguide dimensions. **b**, Broadband dual-comb spectrum obtained with two chirped waveguide PPLNs. The covered span is $1,640\text{ cm}^{-1}$ ($2,250\text{--}3,890\text{ cm}^{-1}$), corresponding to 245,000 teeth at 200 MHz resolution. Also shown is the DCS transmission after performing a baseline correction. Finally, the bottom panels show details of the transmission: the broad spectral span covered within one single measurement allows the simultaneous detection of multiple species, as shown for CO_2 , CH_4 and H_2O . A model based on HITRAN (red trace) matches the measurement well. The noise visible around $3,600\text{ cm}^{-1}$ comprises uncorrected etalon fringes. The occasional noise spikes elsewhere correlate with narrow dips in comb light.

and thereby further decreasing the size of the already compact DCS to enable future portable applications.

Methods

Methods, including statements of data availability and any associated accession codes and references, are available at <https://doi.org/10.1038/s41566-018-0114-7>.

Received: 15 August 2017; Accepted: 29 January 2018;

Published online: 19 March 2018

References

- Coddington, I., Newbury, N. & Swann, W. Dual-comb spectroscopy. *Optica* **3**, 414–426 (2016).
- Ideguchi, T. Dual-comb spectroscopy. *Opt. Photon. News* **28**, 32–39 (2017).
- Boudreau, S., Levasseur, S., Perilla, C., Roy, S. & Genest, J. Chemical detection with hyperspectral lidar using dual frequency combs. *Opt. Express* **21**, 7411–7418 (2013).
- Schroeder, P. J. et al. Dual frequency comb laser absorption spectroscopy in a 16 MW gas turbine exhaust. *Proc. Combust. Inst.* **36**, 4565–4573 (2017).
- Waxman, E. M. et al. Intercomparison of open-path trace gas measurements with two dual-frequency-comb spectrometers. *Atmos. Meas. Tech.* **10**, 3295–3311 (2017).
- Cossel, K. C. et al. Open-path dual-comb spectroscopy to an airborne retroreflector. *Optica* **4**, 724–728 (2017).
- Roy, J., Deschênes, J.-D., Potvin, S. & Genest, J. Continuous real-time correction and averaging for frequency comb interferometry. *Opt. Express* **20**, 21932–21939 (2012).
- Zolot, A. M. et al. Direct-comb molecular spectroscopy with accurate, resolved comb teeth over 43 THz. *Opt. Lett.* **37**, 638–640 (2012).
- Ideguchi, T., Poisson, A., Guelachvili, G., Picqué, N. & Hänsch, T. W. Adaptive real-time dual-comb spectroscopy. *Nat. Commun.* **5**, 3375 (2014).
- Okubo, S. et al. Ultra-broadband dual-comb spectroscopy across 1.0–1.9 μm . *Appl. Phys. Express* **8**, 082402 (2015).
- Schliesser, A., Brehm, M., Keilmann, F. & van der Weide, D. Frequency-comb infrared spectrometer for rapid, remote chemical sensing. *Opt. Express* **13**, 9029–9038 (2005).
- Bernhardt, B. et al. Mid-infrared dual-comb spectroscopy with 2.4 μm Cr^{2+} :ZnSe femtosecond lasers. *Appl. Phys. B* **100**, 3–8 (2010).
- Baumann, E. et al. Spectroscopy of the methane ν_3 band with an accurate midinfrared coherent dual-comb spectrometer. *Phys. Rev. A* **84**, 062513 (2011).
- Schliesser, A., Picqué, N. & Hänsch, T. W. Mid-infrared frequency combs. *Nat. Photon.* **6**, 440–449 (2012).
- Zhang, Z., Gardiner, T. & Reid, D. T. Mid-infrared dual-comb spectroscopy with an optical parametric oscillator. *Opt. Lett.* **38**, 3148–3150 (2013).
- Villares, G., Hugi, A., Blaser, S. & Faist, J. Dual-comb spectroscopy based on quantum-cascade-laser frequency combs. *Nat. Commun.* **5**, 5192 (2014).
- Zhu, F. et al. Mid-infrared dual frequency comb spectroscopy based on fiber lasers for the detection of methane in ambient air. *Laser Phys. Lett.* **12**, 095701 (2015).
- Jin, Y., Cristescu, S. M., Harren, F. J. M. & Mandon, J. Femtosecond optical parametric oscillators toward real-time dual-comb spectroscopy. *Appl. Phys. B* **119**, 65–74 (2015).
- Cruz, F. C. et al. Mid-infrared optical frequency combs based on difference frequency generation for molecular spectroscopy. *Opt. Express* **23**, 26814–26824 (2015).
- Yan, M. et al. Mid-infrared dual-comb spectroscopy with electro-optic modulators. *Light Sci. Appl.* **6**, e17076 (2017).
- Yu, M. et al. Silicon-chip-based mid-infrared dual-comb spectroscopy. Preprint at <http://arxiv.org/abs/1610.01121> (2016).
- Smolski, V. O., Yang, H., Xu, J. & Vodopyanov, K. L. Massively parallel dual-comb molecular detection with subharmonic optical parametric oscillators. Preprint at <http://arxiv.org/abs/1608.07318> (2016).
- Westberg, J., Sterczewski, L. A. & Wysocki, G. Mid-infrared multiheterodyne spectroscopy with phase-locked quantum cascade lasers. *Appl. Phys. Lett.* **110**, 141108 (2017).
- Kara, O., Zhang, Z., Gardiner, T. & Reid, D. T. Dual-comb mid-infrared spectroscopy with free-running oscillators and absolute optical calibration from a radio-frequency reference. *Opt. Express* **25**, 16072–16082 (2017).
- Sinclair, L. C. et al. Invited Article: A compact optically coherent fiber frequency comb. *Rev. Sci. Instrum.* **86**, 081301 (2015).
- Erny, C. et al. Mid-infrared difference-frequency generation of ultrashort pulses tunable between 3.2 and 4.8 μm from a compact fiber source. *Opt. Lett.* **32**, 1138–1140 (2007).
- Maser, D. L., Ycas, G., Depetri, W. I., Cruz, F. C. & Diddams, S. A. Coherent frequency combs for spectroscopy across the 3–5 μm region. *Appl. Phys. B* **123**, 142 (2017).
- Villares, G. et al. On-chip dual-comb based on quantum cascade laser frequency combs. *Appl. Phys. Lett.* **107**, 251104 (2015).
- Truong, G.-W. et al. Accurate frequency referencing for fieldable dual-comb spectroscopy. *Opt. Express* **24**, 30495–30504 (2016).
- Deschênes, J.-D., Giaccarri, P. & Genest, J. Optical referencing technique with CW lasers as intermediate oscillators for continuous full delay range frequency comb interferometry. *Opt. Express* **18**, 23358–23370 (2010).
- Coddington, I., Swann, W. C. & Newbury, N. R. Coherent dual-comb spectroscopy at high signal-to-noise ratio. *Phys. Rev. A* **82**, 043817 (2010).
- Jacobsen, M., Richmond, D., Hogains, M. & Kastner, R. RIFFA 2.1: A Reusable Integration Framework for FPGA Accelerators. *ACM Trans. Reconfigurable Technol. Syst.* **8**, 22 (2015).
- Malathy Devi, V. et al. A multispectrum analysis of the ν_1 band of $\text{H}_2\text{C}_{14}\text{N}$: Part I. Intensities, self-broadening and self-shift coefficients. *J. Quant. Spectrosc. Radiat. Transf.* **82**, 319–341 (2003).
- Rinsland, C. P. et al. A multispectrum analysis of the ν_1 band of $\text{H}_2\text{C}_{14}\text{N}$: Part II. Air- and N_2 -broadening, shifts and their temperature dependences. *J. Quant. Spectrosc. Radiat. Transf.* **82**, 343–362 (2003).
- Moore, C. W., Zielinska, B., Pétron, G. & Jackson, R. B. Air impacts of increased natural gas acquisition, processing, and use: a critical review. *Environ. Sci. Technol.* **48**, 8349–8359 (2014).
- Beale, C. A., Hargreaves, R. J. & Bernath, P. F. Temperature-dependent high resolution absorption cross sections of propane. *J. Quant. Spectrosc. Radiat. Transf.* **182**, 219–224 (2016).
- Newbury, N. R., Coddington, I. & Swann, W. C. Sensitivity of coherent dual-comb spectroscopy. *Opt. Express* **18**, 7929–7945 (2010).

38. Rothman, L. S. et al. The HITRAN 2008 molecular spectroscopic database. *J. Quant. Spectrosc. Radiat. Transf.* **110**, 533–572 (2009).
39. Iwakuni, K. et al. Ortho-para-dependent pressure effects observed in the near infrared band of acetylene by dual-comb spectroscopy. *Phys. Rev. Lett.* **117**, 143902 (2016).
40. Mörz, F. et al. Nearly diffraction limited FTIR mapping using an ultrastable broadband femtosecond laser tunable from 1.33 to 8 μm . *Opt. Express* **25**, 32355–32363 (2017).
41. Hugli, A. Single-shot microsecond mid-infrared spectroscopy with quantum cascade laser frequency combs. In *Optics and Photonics for Energy and the Environment ETu1B.1* (OSA, 2017).
42. Schroeder, P. J. et al. Broadband, high-resolution investigation of advanced absorption line shapes at high temperature. *Phys. Rev. A* **96**, 022514 (2017).

Acknowledgements

The authors acknowledge funding from the Defense Advanced Research Projects Agency Defense Sciences Office SCOUT program, discussions with F. Cruz regarding the design of the lithium niobate waveguides, and helpful comments from A. Fleisher and E. Waxman.

Author contributions

The experiments were conceived of by N.R.N., I.C., G.Y. and S.A.D. The mid-infrared systems were built by G.Y., E.B. and D.H. The digital signal processing was implemented by G.Y. and F.R.G. Data analysis was performed by F.R.G. and G.Y. The manuscript was written by G.Y., F.R.G., I.C. and N.R.N.

Competing interests

The authors declare no competing interests.

Additional information

Supplementary information is available for this paper at <https://doi.org/10.1038/s41566-018-0114-7>.

Reprints and permissions information is available at www.nature.com/reprints.

Correspondence and requests for materials should be addressed to G.Y.

Publisher's note: Springer Nature remains neutral with regard to jurisdictional claims in published maps and institutional affiliations.

Methods

Digital signal processing. Real-time phase correction through digital signal processing has only been demonstrated so far in a relatively narrow optical region around a pair of c.w. lasers acting as transfer oscillators^{29,30}. Here, we generalize the digital signal-processing approach to support broadband DCS by allowing for the correction of a DCS signal at any colour using an arbitrary pair of optical references.

We require the underlying combs obey the standard comb equation, where the phase of the n th mode is

$$\theta_n(t) = n\theta_1(t) + \theta_0(t) \quad (2)$$

and $\theta_1(t) = 2\pi f_r t + \delta\theta_1(t)$ and $\theta_0(t) = 2\pi f_0 t + \delta\theta_0(t)$ in terms of the usual repetition frequency f_r and offset frequency f_0 , and where we allow for phase noise on the comb's repetition rate and offset frequency, $\delta\theta_1(t)$ and $\delta\theta_0(t)$. In DCS, many pairs of modes are simultaneously mixed on a square-law photodetector to generate a series of DCS radiofrequency modes, each with phase

$$\phi_k(t) = k\phi_1(t) + \phi_0(t) \quad (3)$$

where k is the index of a radiofrequency DCS mode and

$$\begin{aligned} \phi_1(t) &= 2\pi\Delta f_r t + \Delta\delta\theta_1(t) \\ \phi_0(t) &\approx 2\pi\Delta f_0 t + n_0\phi_1(t) + \Delta\delta\theta_0(t) - 2\pi m f_{r,\text{comb1}} t \\ \text{where} \\ \Delta f_r &= f_{r,\text{comb2}} - f_{r,\text{comb1}}, \quad \Delta\delta\theta_r = \delta\theta_{r,\text{comb2}} - \delta\theta_{r,\text{comb1}}, \\ \Delta f_0 &= f_{0,\text{comb2}} - f_{0,\text{comb1}}, \quad \Delta\delta\theta_0 = \delta\theta_{0,\text{comb2}} - \delta\theta_{0,\text{comb1}}. \end{aligned} \quad (4)$$

n_0 is the optical comb-mode index for comb 2 corresponding to the radiofrequency DCS mode when $k=0$. The difference in repetition rates is chosen such that $f_{r,\text{comb1}}/\Delta f_r$ is an integer and $m \equiv \text{round}(n_0\Delta f_r/f_{r,\text{comb1}})$ is present because a DCS signal is typically measured at radiofrequencies between 0 and $f_r/2$ and in many cases $n_0\Delta f_r > f_r/2$. Thus, the measured signal is the heterodyne of modes n from comb 2 with modes $n+m$ from comb 1.

The DCS spectrum loses coherence if the phase noise on its k th mode, $\delta\phi_k(t) = (n_0+k)\Delta\delta\theta_1(t) + \Delta\delta\theta_0(t)$, exceeds a radian, leading to a loss in SNR as $\exp(-\langle\delta\phi_k^2\rangle)$. Moreover, if the phase noise extends across neighbouring modes, the comb tooth resolution is lost and, with it, the frequency resolution and accuracy that distinguishes DCS from FTS. To avoid this decoherence, we correct the DCS interferogram signal in the time domain, assuming knowledge of $\Delta\delta\theta_r$ and $\Delta\delta\theta_0$. First, we rotate the phase of the digitized interferogram by $-\phi_0(t)$. Second, the timing variations are removed by resampling the recorded interferogram by linear interpolation onto a new time axis, determined by

$$t' = t + \Delta\delta\theta_1(t)/2\pi f_r \quad (5)$$

To perform these corrections, it is necessary to measure $\theta_1(t)$ and $\theta_0(t)$ for each mid-infrared comb with sufficient precision to evaluate $\delta\phi_k(t)$ to much better than 1 rad. Our mid-infrared light is generated using DFG, and consequently the mid-infrared combs have $f_0 = \delta\theta_0 = 0$. However, we must measure $\Delta\delta\theta_r$ with sufficient precision such that $(n_0+k)\Delta\delta\theta_r$ is much less than 1 rad at short (tens of microseconds) timescales. To reach this precision via direct measurements of the mid-infrared combs' repetition-rate signal is extremely demanding and has not yet been demonstrated. Instead, we extract this quantity from measurements of the near-infrared combs as follows. The near-infrared $\theta_0(t)$ is measured using an $f-2f$ interferometer. A second measurement of each near-infrared comb's phase is made by beating the n_{opt} mode near 1,560 nm against a common c.w. laser, providing a phase signal $\delta\theta_{\text{opt}}(t)$. The difference $\Delta\delta\theta_{\text{opt}}(t) \equiv \delta\theta_{\text{opt,comb2}}(t) - \delta\theta_{\text{opt,comb1}}(t)$ is calculated, removing dependence on the c.w. laser's phase, and finally we calculate $\Delta\delta\theta_1(t) = n_{\text{opt}}^{-1}[\Delta\delta\theta_{\text{opt}}(t) - \Delta\delta\theta_0(t)]$.

In an extension of earlier work^{27,30}, we implement the phase-correction algorithm using standard signal-processing techniques in real time on a FPGA. The radiofrequency signals from each of the near-infrared combs' two locks—in our case f_0 beat notes (via self-referencing) and at 1,560 nm (against a c.w. laser)—and the interferogram are digitized with a 14 bit analog-to-digital converter that is clocked on comb 1's repetition rate. These real signals are converted to complex

ones using in-phase and quadrature (IQ) demodulation, and the phase errors are calculated using the arctangent operation implemented using a CORDIC. From these phase error signals, point-by-point phase and timing corrections to the mid-infrared DCS signals are computed from the above equations using fixed-point arithmetic and applied to the DCS signal by multiplication with a complex phasor and linear interpolation, respectively. Here, the near-infrared frequency combs are sufficiently tightly phase-locked that the timing resampling is unnecessary, provided that the phasor is computed not by $\phi_0(t)$, but instead by $\delta\phi_k(t)$, where mode k is centred in the mid-infrared DCS spectrum.

This high-bandwidth, real-time phase correction compensates for phase noise originating with the near-infrared combs. To compensate for additional slow drifts in timing and phase from optical path length variations in the amplification, DFG set-up and optical cell, a cross-correlator is implemented on the FPGA that compares the stream of interferograms to a reference interferogram. The position and phase of the cross-correlation peaks are used as error signals for proportional-integral feedback to the real-time phase and timing correction processor⁷, which 'locks' the timing and phase offsets to zero on a timescale of about 10 interferograms, here compensating for noise slower than 10 Hz.

In addition to the real-time phase correction, the FPGA signal processor also implements coherent averaging. Coherent averaging is critical to reducing the data size for any reasonable averaging time³¹. A single interferogram, up to ~8 million points long, is buffered in dynamic random-access memory (DRAM.) After phase/timing corrections, subsequent interferograms are added point by point to this interferogram and written back to the buffer. This process can be repeated to average up to 65,000 interferograms on the FPGA, at which point they are transmitted to the PC over the RIFFA interface³².

Coherent averaging and figure of merit. We define the noise as the 'spectral noise', or the standard deviation of the dual-comb spectrum after broad features are removed by high-pass filtering the Fourier-transformed interferogram. We then calculate the figure of merit³⁷ by extending the expression

$$\text{FOM} = m \times \text{SNR} / \sqrt{t} \quad (6)$$

so that we can account for the variation in SNR across the spectrum. Our figure of merit averages the SNR across the modes and is defined as

$$\text{FOM} = \sum_{n=n_{\text{low}}}^{n_{\text{high}}} \frac{I_n}{\sqrt{t}\sigma_n} \quad (7)$$

where n_{low} and n_{high} are the indices of the lowest and highest frequency spectral elements in the dual-comb spectrum, I_n is the signal strength of each element, and σ_n is the one-sigma deviation at mode n .

As assumed in this expression, a dual-comb spectrometer using coherent averaging should exhibit a SNR that increases with the square root of the number of averages, or time. We have verified this scaling in our system. In one of our measurements we recorded both 600 ms of continuous data as well as averaged data of up to $N=100,000$ interferograms, recorded as ten consecutive sets of 10,000 averages each. From these data, we calculate the spectral SNR as a function of averaging time over five orders of magnitude. As shown in Supplementary Fig. 1, the peak SNR increases as a function of \sqrt{N} as expected, in this case increasing by $8.1/\sqrt{N}$.

Alternate configuration of waveguides. While producing broadband optical spectra from the aperiodically poled lithium niobate waveguides it became apparent that our 25-mm-long waveguides provided an interaction length that was too long for the generation of smooth optical spectra. We therefore cut one of our waveguides, keeping just the first 10 mm with poling period ranging from 32 to 26 μm . Using this short waveguide, a DFG spectrum that is smooth and with 90 mW of average power could be generated, as shown in Supplementary Fig. 2. Using a 15 mm focal length off-axis paraboloid (OAP) mirror to collimate the light leaving the waveguide and a 15 mm focal length OAP mirror to focus light into a single-mode ZrF₄ fibre, a maximum of 30 mW was coupled into the fibre.

Data availability. The data that support the plots within this paper and other findings of this study are available from the corresponding author upon reasonable request.